Metal-Insulator Transitions and Realistic Modelling of Correlated Electron Systems

N. Blümer[1], K. Held[2], G. Keller, and D. Vollhardt

Theoretische Physik III, Elektronische Korrelationen und Magnetismus, Institut für Physik
Universität Augsburg, 86135 Augsburg, Germany

[1] Present address: Institut für Physik, Universität Mainz, 65099 Mainz, Germany
[2] Present address: Physics Department, Princeton University, Princeton, NJ 08544, USA

The correlation-induced metal-insulator transition found experimentally in Cr-doped V_2O_3 is investigated within the one-band Hubbard-type model and a realistic multi-band model, using dynamical mean-field theory (DMFT). The DMFT equations are solved numerically with an auxiliary-field quantum Monte-Carlo algorithm. For the one-band model a detailed phase diagram is obtained which resolves a long-standing controversy. The calculated spectra, orbital occupations and the spin state obtained for the realistic model are found to agree with recent polarization dependent X-ray-absorption experiments.

1 Introduction

The calculation of physical properties of electronic systems by controlled approximations is one of the most important challenges of modern theoretical solid state physics. In particular, the physics of transition metal oxides – a singularly important group of materials both from the point of view of fundamental research and technological applications – may only be understood by explicit consideration of the strong effective interaction between the conduction electrons in these systems. The investigation of electronic many-particle systems is made especially complicated by quantum statistics, and by the fact that the phenomena of interest (e.g., metal insulator transitions and ferromagnetism) usually require the application of non-perturbative theoretical techniques.

One of the most famous examples of a cooperative electronic phenomenon of this type is the transition between a paramagnetic metal and a paramagnetic insulator induced by the Coulomb interaction between the electrons, referred to as Mott-Hubbard metal-insulator transition. The question concerning the nature of this transition poses one of the fundamental theoretical problems in condensed matter physics.[1,2] Correlation-induced metal-insulator transitions (MIT) are found, for example, in transition metal oxides with partially filled bands near the Fermi level. For such systems band theory typically predicts metallic behavior. The most famous example is V_2O_3 doped with Cr;[3–5] see Fig. 1. While at low temperatures V_2O_3 is an antiferromagnetic insulator with monoclinic crystal symmetry, it has a corundum structure with a small trigonal distortion in the high-temperature paramagnetic phase. All transitions shown in the phase diagram (Fig. 1) are of first order. In the case of the transitions from the high-temperature paramagnetic phases into the low-temperature antiferromagnetic phase this is naturally explained by the fact that the transition is accompanied by a change in crystal symmetry. By contrast, the crystal symmetry across the MIT in the paramagnetic phase remains intact, since only the ratio of the c/a axes changes discontinuously. This was usually taken as an indication for the predominantly electronic origin of this MIT.
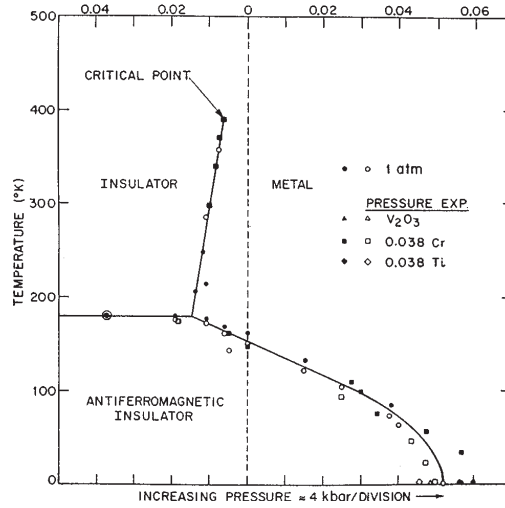
Figure 1. Phase Diagram of V_2O_3 doped with Cr or Ti (temperature versus external pressure); from Ref. 4.

2 One-Band Hubbard Model

To explain a MIT induced by electronic correlations one may choose to start with the investigation of an electronic many-body model to understand, at least, some of the basic features of the MIT, or employ more material-specific approaches. Concerning the former approach,[5,1] the spin $S = 1/2$, half-filled, single-band Hubbard model,[6–8]

$$\hat{H}_{\text{one-band}} = -t \sum_{\langle i,j \rangle, \sigma} \left(\hat{c}_{i\sigma}^\dagger \hat{c}_{j\sigma} + \hat{c}_{j\sigma}^\dagger \hat{c}_{i\sigma} \right) + U \sum_i \hat{n}_{i\uparrow} \hat{n}_{i\downarrow} , \qquad (1)$$

is certainly the simplest possible model to be investigated. Here, the operators $\hat{c}_{i\sigma}^\dagger$ and $\hat{c}_{i\sigma}$ create and annihilate electrons of spin σ on lattice site i, respectively, while $\hat{n}_{i\sigma} = \hat{c}_{i\sigma}^\dagger \hat{c}_{i\sigma}$ counts the electrons of spin σ on site i. It should be noted that due to the Pauli principle a lattice site can be occupied by at most one electron per spin species $\sigma \in \{\uparrow, \downarrow\}$. While the on-site interaction energy parametrized by U is diagonal in the *real*-space representation (1), the kinetic energy, i.e., the hopping processes parametrized by t, is diagonal in *momentum* space. Thus the two terms in the Hamiltonian are maximally incompatible concerning their commutation.

The existence of a MIT in the paramagnetic phase[9] of the half-filled Hubbard model had been investigated already in the early work of Hubbard.[10] The details of the transition remained unclear for a long time. During the last few years, however, our understanding of the MIT in the one-band Hubbard model has considerably improved due to the application of the dynamical mean-field theory (DMFT). Within the DMFT, the electronic lattice problem is mapped onto a single-impurity Anderson model (SIAM) with a self-consistency condition. The mapping becomes exact in the limit of infinite coordination number[11,12] and allows one to investigate the dynamics of correlated lattice electrons non-perturbatively at all interaction strengths. This is of essential importance for a problem like the MIT which
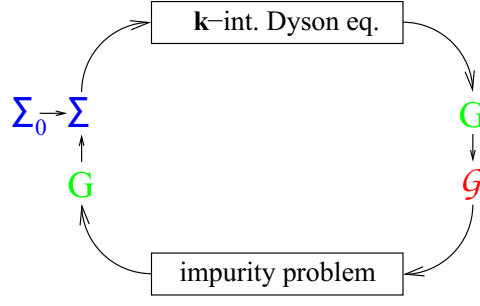
Figure 2. DMFT self-consistency cycle (see text).

occurs at a Coulomb interaction comparable to the electronic band-width. The Green function for the SIAM can be written as a functional integral over Grassmann variables ψ, ψ^*,

$$G_{\sigma n} = -\langle \psi_{\sigma n} \psi_{\sigma n}^* \rangle_{\mathcal{A}} = -\frac{1}{\mathcal{Z}} \int \mathcal{D}[\psi]\mathcal{D}[\psi^*]\, \psi_{\sigma n} \psi_{\sigma n}^*\, e^{\mathcal{A}[\psi,\psi^*,\mathcal{G}]}\,. \tag{2}$$

Here, the index n denotes the fermionic Matsubara frequency $\omega_n = (2n+1)\pi T$ for temperature T and $\mathcal{Z}$ is the partition function

$$\mathcal{Z} = \int \mathcal{D}[\psi]\mathcal{D}[\psi^*]\, e^{\mathcal{A}[\psi,\psi^*,\mathcal{G}]}\,. \tag{3}$$

The action $\mathcal{A}$ can be expressed as $\mathcal{A}[\psi,\psi^*,\mathcal{G}] = \lim_{\Lambda \to \infty} \mathcal{A}_\Lambda[\psi,\psi^*,\mathcal{G}]$ in terms of a discretized imaginary time $\tau_l = l\Delta\tau$ with a finite number $\Lambda = \beta/\Delta\tau$ of time slices, where $\beta = 1/T$ is the inverse temperature and

$$\mathcal{A}_\Lambda[\psi,\psi^*,\mathcal{G}] = (\Delta\tau)^2 \sum_\sigma \sum_{l,l'=0}^{\Lambda-1} \psi_{\sigma l}^* (\boldsymbol{\mathcal{G}}_\sigma^{-1})_{ll'} \psi_{\sigma l'} - \Delta\tau U \sum_{l=0}^{\Lambda-1} \psi_{\uparrow l}^* \psi_{\uparrow l} \psi_{\downarrow l}^* \psi_{\downarrow l}\,. \tag{4}$$

The self consistency requires that the impurity Green function, which is related to the (local) self energy Σ by the impurity Dyson equation $\mathcal{G}_{\sigma n}^{-1} = G_{\sigma n}^{-1} + \Sigma_{\sigma n}$, also fulfills the **k** integrated lattice Dyson equation,

$$G_{\sigma n} = \int_{-\infty}^{\infty} d\varepsilon\, \frac{\rho_0(\varepsilon)}{i\omega_n + \mu - \Sigma_{\sigma n} - \varepsilon}\,. \tag{5}$$

This equation is essential since it introduces the lattice nature of the problem via the non-interacting density of states $\rho_0(\epsilon)$. A numerical solution of the DMFT problem is achieved in an iterative process as illustrated in Fig. 2. Starting with some initial self energy Σ_0, (5) is used to calculate the bath Green function $\mathcal{G}$ which defines the impurity problem. Its solution is a difficult problem which is in this work achieved using the auxiliary-field quantum Monte Carlo (QMC) algorithm by Hirsch and Fye.[13] After a Trotter decomposition of $e^{\mathcal{A}}$, a discrete Hubbard-Stratonovich transformation is employed,

$$\exp\left(\frac{\Delta\tau U}{2}(\psi_{\uparrow l}^* \psi_{\uparrow l} - \psi_{\downarrow l}^* \psi_{\downarrow l})^2\right) = \frac{1}{2} \sum_{s_l = \pm 1} \exp\left(\lambda s_l(\psi_{\uparrow l}^* \psi_{\uparrow l} - \psi_{\downarrow l}^* \psi_{\downarrow l})\right) \tag{6}$$

349

with $\cosh \lambda = \exp(\Delta\tau U/2)$. Thus, the electron-electron interaction term which is quartic in the Grassmann variables is replaced by the interaction with an external auxiliary Ising field $\{s_l\}$ with $s_l = \pm 1$. For a given Ising configuration, the functional integral becomes

$$G_{\sigma ll'} = \frac{1}{\mathcal{Z}} \sum_{\{s_i\}} \left(\mathbf{M}_\sigma^{\{s_i\}}\right)_{ll'}^{-1} \det \mathbf{M}_\uparrow^{\{s_i\}} \det \mathbf{M}_\downarrow^{\{s_i\}}, \qquad (7)$$

where $\boldsymbol{M}_\sigma^{\{s_i\}}$ is the matrix with elements $M_{\sigma ll'}^{s_l} = (\Delta\tau)^2 (\boldsymbol{\mathcal{G}}_\sigma^{-1})_{ll'} - \lambda\sigma\delta_{ll'} s_l$, and the partition function has the value

$$\mathcal{Z} = \sum_{\{s_i\}} \det \mathbf{M}_\uparrow^{\{s_i\}} \det \boldsymbol{M}_\downarrow^{\{s_i\}}. \qquad (8)$$

Computing one of the 2^Λ terms in (7) directly is an operation of order $\mathcal{O}(\Lambda^3)$. However, if the terms are ordered in a way so that successive configurations $\{s_i\}$ and $\{s_i\}'$ only differ by one flipped spin $s_l \to -s_l$ then all matrices and determinants can be updated at a cost of $O(\Lambda^2)$.[14] Only for $\Lambda \lesssim 24$ can all terms be summed up exactly. Computations at larger Λ are made possible by Monte Carlo importance sampling which drastically reduces the number of terms that have to be calculated explicitly from 2^Λ to order $O(\Lambda)$. Here, the absolute values of the products of determinants in (7) and (8) are used as unnormalized probabilities in a Metropolis single-spin update Markov chain. Numerical errors arise at several stages of the algorithm: The finite Monte Carlo sampling length introduces a statistical error (and possibly a systematic error from incomplete warm-up); systematic errors incur from the finite number of iteration cycles and, most importantly, the finite discretization $\Delta\tau$ of the imaginary time. For constant accuracy, i.e., for a constant value of $\Delta\tau$ and constant numbers of iterations and sweeps, the total numerical effort scales with T^{-3}, i.e., rapidly increases with decreasing temperature. In the one-band calculations discussed in this section, very high accuracy could be obtained even at low temperatures by using up to 10^6 sweeps per iteration, about 10-100 iterations, and up to $\Lambda_{max} = 400$ time slices.

The DMFT provides a framework for deriving a coherent picture of the electronic spectrum at all energy scales, i.e., of the incoherent features at high energies (Hubbard bands),[10] and the coherent quasi-particle behavior at low energies.[7,15] At $T = 0$ the transition from the metallic to the insulating state is then signaled by the collapse of the Fermi liquid quasi-particle peak at the Fermi energy when the interaction is increased.[16] Qualitatively, this behavior is still seen at finite, not too high temperatures as shown in Fig. 3 for $T = 0.05$. When the interaction U becomes of the order of the noninteracting bandwidth $W = 4$, weight is shifted from the quasi-particle peak at $\omega \approx 0$ to the upper and lower Hubbard bands. Within the Fermi liquid regime ($U \lesssim 4.4$), the DOS at the Fermi energy ($\omega = 0$) is essentially pinned to its noninteracting value. The deviation for $U = 4.7$ signals the breakdown of the Fermi liquid before the MIT occurs at $U \approx 4.8$. The insulating gap becomes more pronounced and widens when the interaction is further increased.

Spectra as shown in Fig. 3 require analytic continuation to the real axis via a maximum-entropy method[17] which is quantitatively less reliable than the QMC procedure itself. Therefore, the phase diagram can be much more accurately determined from the analysis of static properties. In Fig. 4a, the total energy E per lattice site is shown for a relatively high temperature $T = 0.067$ as a function of U. For each value of the discretization $\Delta\tau$, a
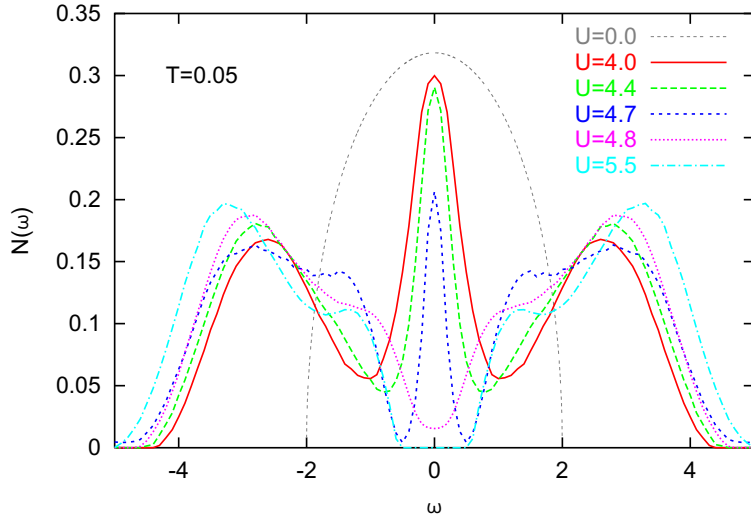
Figure 3. Spectra of the half-filled one-band Hubbard model for discretization $\Delta\tau = 0.1$.
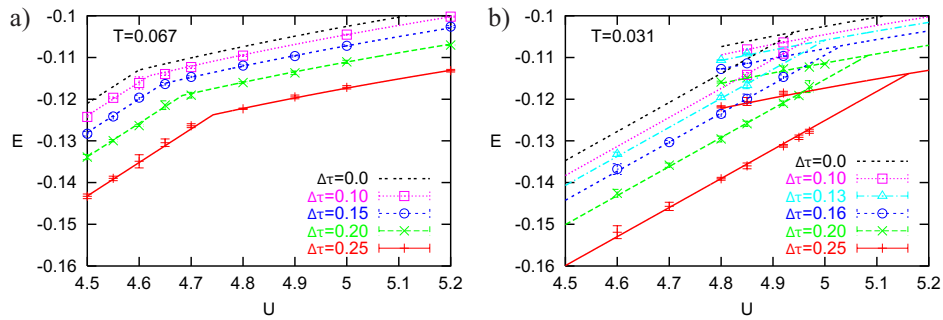

Figure 4. Energy E per lattice site as a function of on-site interaction U for (a) $T = 0.067$, and (b) $T = 0.031$. Both figures show results for finite discretization $\Delta\tau$ and extrapolations to the physical limit $\Delta\tau = 0$.

kink clearly signals the metal-insulator transition. Due to the regular shape, it is also possible to extrapolate to the physical limit $\Delta\tau \to 0$. At the lower temperature $T = 0.031$, one finds hysteresis between metallic and insulating solutions which coexist for $4.8 \lesssim U \lesssim 5.0$ (depending on $\Delta\tau$) as seen in Fig. 4b. This coexistence points to a first-order transition at low temperatures in qualitative agreement with the respective transition observed in V_2O_3. The crosses in the phase diagram (Fig. 5) summarize the QMC measurements of crossover lines, the transition point, and the coexistence region above, at, and below the critical temperature $T^* \approx 0.067$, respectively. These results show excellent agreement with recent finite-temperature calculations[18] using the numerical renormalization group (NRG) to solve the DMFT equations, but deviate considerably from early estimates[12] obtained within iterated perturbation theory (IPT). Obviously, the first-order phase transition line has to be pinpointed within the coexistence region for obtaining the full phase diagram. While a direct comparison of free energies is numerically unstable, we succeeded in deter-
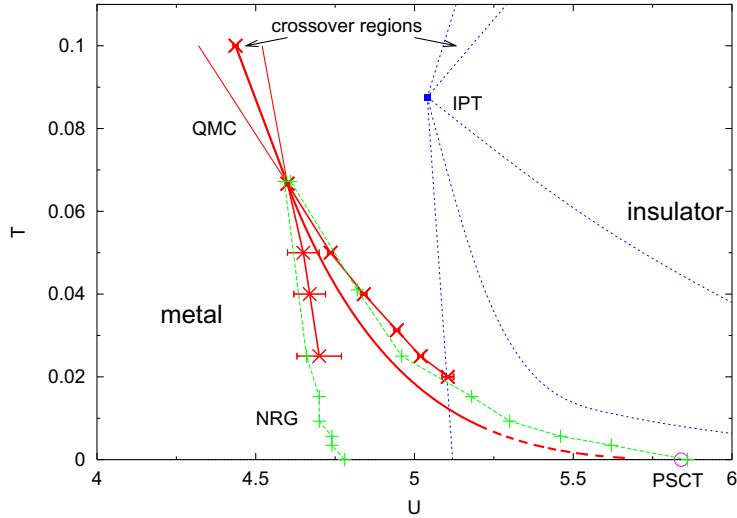
Figure 5. Phase diagram of the half-filled one-band Hubbard model in the paramagnetic phase. QMC results (crosses and thick lines) are compared with NRG (squares) and IPT (dotted lines) results. The first-order transition line extrapolates to the point at $T \rightarrow 0$ obtained by the projective self-consistent theory (PSCT)[12].

mining the first-order transition line from a Clausius-Clapeyron differential equation using very precise measurements of energy and double occupancy plus low-temperature Fermi liquid properties. The corresponding thick curve in Fig. 5 is drawn as a solid line where it is completely determined from QMC, and as a dashed line at low temperatures where it is dominated by additional (reliable) input from ground state methods such as NRG[18] and the projective self-consistent theory (PSCT)[12]. The precise determination of the phase diagram Fig. 5 does not only resolve a long-standing controversy about the physics of the half-filled frustrated one-band Hubbard model within the DMFT, but may also serve as a benchmark for alternative numerical methods of solving the DMFT equations.

3 Realistic Model for V_2O_3

Although the Hubbard model is able to explain certain basic features of the Mott-Hubbard MIT and the phase diagram of V_2O_3, it cannot explain the physics of that material in any detail. Clearly, a realistic theory of V_2O_3 must take into account the complicated electronic structure of this system. In the high-temperature paramagnetic phase V_2O_3 has an electronic structure with a $3d^2$ V^{3+} state, where the two e_g-orbitals are empty and the three t_{2g}-orbitals are filled with two electrons. A small trigonal distortion lifts the triple degeneracy of the t_{2g}-orbitals, resulting in one non-degenerate a_{1g}-orbital and two degenerate e_g^π orbitals. Starting from this orbital structure Castellani et $al.$[19] proposed a widely accepted model with a strong covalent a_{1g}-bond between two V ions along the c-axis. This bonding state is occupied by a singlet pair (one electron per V) and hence does not contribute to the local magnetic moment. The remaining electron per V has a twofold orbital degeneracy within the e_g^π orbitals and a spin $S = 1/2$. This $S = 1/2$ model, derived

within a material-specific approach, strongly supported the hope that the half filled, one-band Hubbard model was not only the simplest possible, but, in fact, a valid starting point for the investigation of V_2O_3.

However, recent experimental results by Park *et al.*[20] seem to require an interpretation in terms of a $S = 1$ spin state, and an $e_g^\pi e_g^\pi$ orbital state with an admixture of $e_g^\pi a_{1g}$ configurations. Subsequently, Ezhov *et al.*[21] and Mila *et al.*[22] argued for $S = 1$ models without and with orbital degeneracy, respectively, for the antiferromagnetic insulating phase of V_2O_3. LDA+U calculations indicate that the atomic Hund's rule is responsible for the high-spin ground state of the V ions.[21] While LDA+U may be used to describe the antiferromagnetic insulating phase of V_2O_3, the metal-insulator transition within the correlated *paramagnetic* phase is beyond the scope of this approach since the Coulomb interaction is treated within Hartree-Fock. Here the computational scheme LDA+DMFT,[23–26] obtained by combining electronic band structure theory (LDA) with the many-body technique DMFT, is the best available method for the investigation of real systems close to a Mott-Hubbard MIT.[27] To solve the DMFT-equations we[28] employ a multiband-version of the quantum Monte Carlo method[29,30] which yields a numerically exact solution;[31] the resulting calculational scheme is referred to as LDA+DMFT(QMC).[24,26,27] Note that in multiband QMC calculations (with $M = 3$ bands), the numerical cost increases by an additional factor of $2M^2 - M = 15$ compared to the single-band case, so that for a comparable computer allocation the lowest attainable temperature increases by about a factor of 2.5.

In a first step, LDA calculations were performed for paramagnetic *metallic* V_2O_3 and paramagnetic *insulating* $(V_{0.962}Cr_{0.038})_2O_3$, respectively.[28] The LDA results for corundum V_2O_3 and $(V_{0.962}Cr_{0.038})_2O_3$ are very similar. In particular, the changes in crystal and electronic structure occuring at the transition are insufficiently reflected by the LDA calculations and the experimentally observed insulating gap is *missing* in the LDA DOS. It is generally believed that this insulating gap is due to strong Coulomb interactions which are not adequately accounted for by the LDA. This is where our LDA+DMFT(QMC) scheme sets in. Using this approach we can show explicitly that the insulating gap is indeed caused by electronic correlations.

In the LDA+DMFT approach[23–27] the LDA band structure, expressed by a one-particle Hamiltonian H_{LDA}^0, is supplemented with the local Coulomb repulsion U and Hund's rule exchange J:

$$\hat{H} = \hat{H}_{\mathrm{LDA}}^0 + U \sum_m \sum_i \hat{n}_{im\uparrow}\hat{n}_{im\downarrow} + \sum_{i,m\neq\tilde{m},\sigma,\tilde{\sigma}} (V - \delta_{\sigma\tilde{\sigma}}J) \, \hat{n}_{im\sigma}\hat{n}_{i\tilde{m}\tilde{\sigma}}. \quad (9)$$

Here, i denotes the lattice site; m and $\tilde{m}$ enumerate the three interacting t_{2g} orbitals. The interaction parameters are related by $V = U - 2J$ which holds exactly for degenerate orbitals and is a good approximation for the t_{2g} orbitals. Furthermore, since the t_{2g} bands at the Fermi energy are rather well separated from all other bands we restrict the calculation to these bands (for details of the computational scheme see Refs. 26, 27). With this restriction only the LDA DOS of the three t_{2g} bands enter the LDA+DMFT calculation.[27] The LDA-calculated value of the Coulomb repulsion U has a typical uncertainty of at least 0.5 eV.[26] For this reason, we adjust U to yield a metal-insulator transition with Cr doping. *A posteriori*, we can compare whether the adjusted value is in the range of values obtained from a constrained LDA calculation.
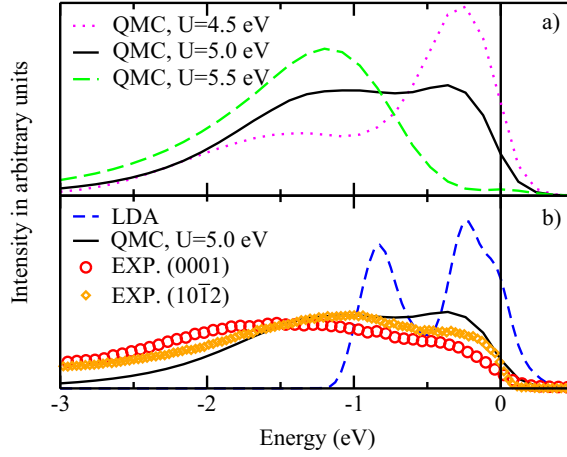
Figure 6. a) LDA+DMFT(QMC) spectrum for $U = 4.5, 5$ and 5.5 eV at $T = 0.1$ eV ≈ 1000 K; b) Comparison with the LDA spectrum and the photoemission experiment by Schramme *et al.*[35] for two different V_2O_3 single-crystal surfaces at $T = 300$ K. Note, that the $(10\bar{1}2)$ surface has the same coordination number as the bulk.

The spectra obtained by LDA+DMFT(QMC) imply that the critical value of U for the MIT is about 5 eV. Indeed, at $U = 4.5$ eV one observes pronounced quasiparticle peaks at the Fermi energy, i.e., characteristic metallic behavior, even for the crystal structure of $(V_{0.962}Cr_{0.038})_2O_3$, while at $U = 5.5$ eV the form of the calculated spectral function is typical for an insulator for both sets of crystal structure parameters. (We note that at $T \approx 0.1$ eV one only observes metallic-like and insulating-like behavior, with a rapid but smooth crossover between these two phases, since a sharp MIT occurs only at lower temperatures.[34, 16])

To compare with the photoemission spectrum of V_2O_3 by Schramme *et al.*,[35] the LDA+DMFT(QMC) spectra are multiplied with the Fermi function at $T = 0.1$ eV and Gauss-broadened by 0.05 eV to account for the experimental resolution. The theoretical results[28] for $U = 5$ eV are seen to be in good agreement with experiment (Fig. 6), in contrast with the LDA results. We also note that the DOS is highly asymmetric with respect to the Fermi energy due to the orbital degrees of freedom. This is in striking contrast to the result obtained with a one-band model. The comparison between our results, the data of Müller *et al.*[36] obtained by X-ray absorption measurements, and LDA in Fig. 7 shows that, in contrast with LDA, our results not only describe the different bandwidths above *and* below the Fermi energy (≈ 6 eV and $\approx 2 - 3$ eV, respectively) correctly, but even resolve the two-peak structure above the Fermi energy.

Particularly interesting are the spin and the orbital degrees of freedom in V_2O_3. We find (not shown) that for $U \gtrsim 3$ eV the squared local magnetic moment $\langle m_z^2 \rangle$ saturates at a value of 4, i.e., there are *two* electrons with the same spin direction in the $(a_{1g}, e_{g1}^\pi, e_{g2}^\pi)$ orbitals.[28] Thus, we conclude that the spin state of V_2O_3 is $S = 1$ throughout the Mott-Hubbard transition region. Our $S = 1$ result agrees with the measurements of Park *et al.*[20] and also with the data for the high-temperature susceptibility.[37] Thus LDA+DMFT(QMC) provides a remarkably accurate microscopic theory of the strongly correlated electrons in
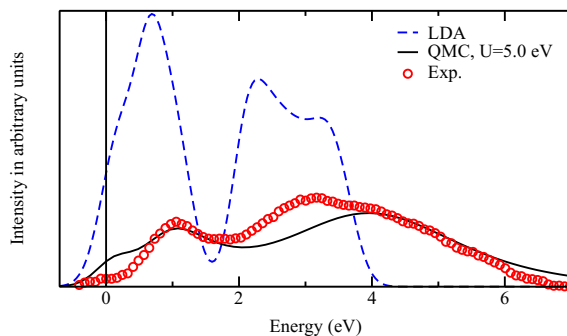
Figure 7. Comparison of the LDA and LDA+DMFT(QMC) spectra at $T = 0.1$ eV (Gaussian broadened with 0.2 eV) with the X -ray absorption data of Müller et al.[36].

the paramagnetic phase of V_2O_3.[28]

The MIT will eventually become first order at lower temperatures;[38, 16] QMC simulations at $T \approx 300$ K are under way, but are very computer-expensive. Furthermore, future investigations will have to clarify the origin of the discontinuous lattice distortion at the first-order MIT which leaves the lattice symmetry unchanged. In particular, the MIT might be the driving force behind the lattice distortion by causing a thermodynamic instability with respect to changes of the lattice volume and distortions.

4   Conclusions

The Mott-Hubbard metal insulator transition is a phenomenon occurring in solids where the effective strength of the Coulomb interaction between the conduction electrons is comparable to the electronic band-width. Thus it belongs to the class of notoriously difficult intermediate coupling problems whose investigation requires non-perturbative techniques. We presented detailed results for the transition scenario occurring in the one-band Hubbard model and in a realistic multi-band model, obtained by the numerical solution of the equations of the dynamical mean-field theory (DMFT) using an auxiliary-field quantum Monte-Carlo algorithm (QMC). Our QMC results provide accurate insight into the details of the Mott-Hubbard metal insulator transition in the one-band model and thereby resolve a long-standing controversy about the nature of this transition. Furthermore, applying the newly developed LDA+DMFT(QMC) scheme, which merges the conventional local density approximation (LDA) with DMFT in combination with QMC, to investigate the paramagnetic phase of V_2O_3 we find remarkable agreement with recent experiments. Indeed, LDA+DMFT(QMC) turns out to be a workable computational scheme which provides, at last, a powerful tool for future *ab initio* investigations of real materials with strong electronic correlations.

The novel computational scheme for the investigation of strongly interacting matter described in this report can only be implemented on vector supercomputers like the CRAY-T90 and massively parallel machines with large caches like the CRAY-T3E of the NIC. In fact, using a total of about 2500 CPU hours on the T90 and 35000 CPU hours on the T3E, the computer simulations reported here already tested the limits of these supercomputers. Eventually a genuine fusion of LDA with DMFT will make it necessary to go to

355

considerable lower temperatures, i.e., room temperature and below. Furthermore, truly realistic investigations of transition metals and their oxides will require the implementation of a scheme where all relevant electronic bands are included. As discussed above a larger number of bands and lower temperatures imply an enormous increase of numerical effort. This shows that substantial progress in the modelling of correlated electronic materials will only be possible with much faster computers. In view of the eminent importance of these materials for fundamental research *and* technological applications the construction and availability of faster supercomputers is thus highly desirable.

Acknowledgments

References

1. N. F. Mott, Rev. Mod. Phys. **40**, 677 (1968); *Metal-Insulator Transitions* (Taylor & Francis, London, 1990).
2. F. Gebhard, *The Mott Metal-Insulator Transition* (Springer, Berlin, 1997).
3. D. B. McWhan and J. P. Remeika, Phys. Rev. **B2**, 3734 (1970).
4. D. B. McWhan *et al.*, Phys. Rev. **B7**, 1920 (1973).
5. T. M. Rice and D. B. McWhan, IBM J. Res. Develop. 251 (May 1970).
6. J. Hubbard, Proc. Roy. Soc. London **A276**, 238 (1963).
7. M. C. Gutzwiller, Phys. Rev. Lett. **10**, 59 (1963).
8. J. Kanamori, Prog. Theor. Phys. **30**, 275 (1963).
9. At low temperatures the paramagnetic phase can be stabilized by appropriately frustrating the incipient antiferromagnetic order in the Hubbard model at half filling.
10. J. Hubbard, Proc. Roy. Soc. London **A281**, 401 (1964).
11. W. Metzner and D. Vollhardt, Phys. Rev. Lett. **62**, 324 (1989).
12. A. Georges, G. Kotliar, W. Krauth, and M. J. Rozenberg, Rev. Mod. Phys. **68**, 13 (1996).
13. J. E. Hirsch and R. M. Fye, Phys. Rev. Lett. **56**, 2521 (1983).
14. R. Blankenbecler, D. J. Scalapino, and R. L. Sugar, Phys. Rev. D **24**, 2278 (1981).
15. W. F. Brinkman and T. M. Rice, Phys. Rev. B **2**, 4302 (1970).
16. G. Moeller, Q. Si, G. Kotliar, M. J. Rozenberg, and D. S. Fisher, Phys. Rev. Lett. **74**, 2082 (1995); J. Schlipf, M. Jarrell, P. G. J. van Dongen, N. Blümer, S. Kehrein, Th. Pruschke, and D. Vollhardt, Phys. Rev. Lett. **82**, 4890 (1999); M. J. Rozenberg, R. Chitra and G. Kotliar, Phys. Rev. Lett. **83**, 3498 (1999); R. Bulla, Phys. Rev. Lett. **83**, 136 (1999).
17. M. Jarrell and J.E. Gubernatis, Physics Reports, **269**, 133 (1996).
18. R. Bulla, T.A. Costi, and D. Vollhardt, Phys. Rev. B **64**, 45103 (2001).
19. C. Castellani, C. R. Natoli, and J. Ranninger, Phys. Rev. B **18**, 4945 (1978); **18**, 4967 (1978); **18**, 5001 (1978).
20. J.-H. Park, L.H. Tjeng, A. Tanaka, J.W. Allen, C.T. Chen, P. Metcalf, J.M. Honig, F.M.F. de Groot, and S.A. Sawatzky, Phys. Rev. B **61**, 11 506 (2000).

21. S. Yu. Ezhov, V. I. Anisimov, D. I. Khomskii, and G. A. Sawatzky, Phys. Rev. Lett. **83**, 4136 (1999).
22. F. Mila, R. Shiina, F.-C. Zhang, A. Joshi, M. Ma, V. Anisimov, and T. M. Rice, Phys. Rev. Lett. **85**, 1714 (2000).
23. V. I. Anisimov, A. I. Poteryaev, M. A. Korotin, A. O. Anokhin, and G. Kotliar, J. Phys.: Cond. Matt. **9**, 7359 (1997).
24. A. I. Lichtenstein and M. I. Katsnelson, Phys. Rev. B **57**, 6884 (1998).
25. M. B. Zölfl, Th. Pruschke, J. Keller, A. I. Poteryaev, I. A. Nekrasov, and V. I. Anisimov, Phys. Rev. B **61**, 12810 (2000).
26. I. A. Nekrasov, K. Held, N. Blümer, A. I. Poteryaev, V. I. Anisimov, and D. Vollhardt, Euro Phys. J. B **18**, 55 (2000).
27. For an introduction into LDA+DMFT, see K. Held, I. A. Nekrasov, N. Blümer, V. I. Anisimov, and D. Vollhardt, Int. J. Mod. Phys. B **15**, 2611 (2001).
28. K. Held, G. Keller, V. Eyert, D. Vollhardt, and V. I. Anisimov, Phys. Rev. Lett. **86**, 5345 (2001).
29. J. E. Han, M. Jarrell, and D. L. Cox, Phys. Rev. B **58**, R4199 (1998).
30. K. Held and D. Vollhardt, Euro. Phys. J. B **5**, 473 (1998).
31. For a comparison of LDA+DMFT results for the photoemission spectra of $La_{1-x}Sr_xTiO_3$ obtained by different numerical techniques see Ref. 26.
32. Use of the crystal structure of Cr-doped V_2O_3 for the insulating phase of pure V_2O_3 is justified by the observation that Cr-doping is equivalent to the application of (negative) pressure.
33. All QMC results presented were obtained for $T = 0.1$ eV. Simulations for V_2O_3 at $U = 5$ eV, $T = 0.143$ eV, and $T = 0.067$ eV suggest, however, only a minor smoothing of the spectrum with increasing temperature.
34. M. J. Rozenberg, Phys. Rev. B **55**, R4855 (1997).
35. M. Schramme, Ph.D. thesis, Universität Augsburg, 2000; M. Schramme *et al.* (unpublished). Recent experiments by H.-D. Kim *et al.* (cond-mat/0108044) which are more sensitive to bulk properties show an even better agreement.
36. O. Müller, J. P. Urbach, E. Goering, T. Weber, R. Barth, H. Schuler, M. Klemm, S. Horn, and M. L. denBoer, Phys. Rev. B **56**, 15056 (1997).
37. D. J. Arnold, R. W. Mires, J. Chem. Phys. **48**, 2231 (1968).
38. M. J. Rozenberg, G. Kotliar, H. Kajueter, G. A. Thomas, D. H. Rapkine, J. M. Honig, and P. Metcalf, Phys. Rev. Lett. **75**,105 (1995).